A Study on Structural and Diffusion Properties of Porcine Stratum Corneum Based on Very Small Angle Neutron Scattering Data

Georgia Ch. Charalambopoulou,[1,2] Panagiotis Karamertzanis,[1] Eustathios S. Kikkinides,[1] Athanassios K. Stubos,[1,3] Nick K. Kanellopoulos,[1] and Agelos Th. Papaioannou[2]

Received May 23, 2000; accepted June 9, 2000

Purpose. Generation of valuable information about the biphasic geometrical configuration of porcine stratum corneum from Very Small Angle Neutron Scattering (VSANS) data and investigation of its effect on the corresponding effective diffusivity.

Methods. Spectra of porcine stratum corneum are mathematically transformed in order to obtain the corresponding auto-correlation function (ACF). Model stratum corneum structures, matching this experimentally determined ACF, are then produced based on the "brick-and-mortar" configuration. The effective diffusivity through these model domains is calculated using an appropriate numerical method.

Results. The most appropriate geometry of porcine stratum corneum's lipid and protein phases in a "brick-and-mortar" configuration is quantitatively determined and correlated with the barrier properties (diffusivity) of the stratum corneum model structures.

Conclusions. The ACF analysis indicates the most appropriate values for the dimensions of the corneocyte thickness and the surrounding lipid gap, while the corneocyte length is estimated from the diffusion study.

KEY WORDS: stratum corneum; structural characteristics; diffusion; neutron scattering.

INTRODUCTION

The aim of transdermal drug delivery is usually for the drug to reach the systemic circulation, either vascular or lymphatic. For passive delivery, this means that there are a number of solubility and diffusional barriers to overcome (1). For most drugs, the rate-limiting steps are partitioning into and diffusion through the stratum corneum (SC), the outermost layer of epidermis (1–3). This owes largely to the fact that SC is composed of densely packed corneocytes, separated by multilamellar lipid bilayers. In combination, the densely packed corneocytes and bilayer lipid regions function to minimize the transdermal transport of both lipophilic and hydrophilic substances. The overall permeability of SC can be quantitatively related to the transport properties of its two phases (i.e., protein and lipid) and to their geometric configuration.

The effective diffusivity of any penetrant through SC should be determined by the following physicochemical parameters: a) D_L and D_P, which represent the specific diffusivity through the lipid and protein phase of the tissue, respectively; and b) the partition coefficient, κ, of the penetrant between the lipid and protein phases. These parameters define the dimensionless factor σ, as the product of the partition coefficient κ, and the quotient D_L/D_P. The permeability of the corneocytes within intact SC is virtually unknown, with opinions varying between fully impermeable (4) and highly permeable (5). This justifies why a D_P value for drugs has never been systematically determined, while scattered estimations possess a high degree of uncertainty (3). On the other hand, few measurements of D_L for drugs, in a mixture of model SC lipids, are available and give values which lie within the range 10^{-9}–10^{-8} cm^2/s, depending on the actual mixture composition (6).

Several mathematical models have been presented attempting to describe, from a macroscopic point of view, the solute transport process and provide estimations for drug permeability through the SC. Michaels *et al.* (7) developed an analytical approximation that includes permeation both paracellularly and transcellularly, by introducing a "brick-and-mortar" geometry for the representation of the actual SC structure. The tissue is postulated to consist of a parallel array of thin plates, each consisting of protein, which are separated from one another by thin layers of lipoidal material. The lipid region is the continuous phase of the matrix, whereas the proteinaceous phase is supposedly discontinuous. Both phases however, are considered homogeneous and isotropic. Later, Tojo (8) attempted to advance this model, using an analytical approach and somehow randomizing the arrangement of the corneocytes within the lipid phase. Since steady state is not always achieved *in vivo,* Albery and Hadgraft (9) developed an unsteady state diffusion model also based on the "brick-and-mortar" geometry. Although an exact solution was not possible, they determined that the route followed by the diffusing solute, depends on the diffusion characteristics of the two phases. Recently, Heisig *et al.* (10) developed a numerical method to solve the time-dependent drug concentration within both SC phases. They concluded that the very small experimental permeability values reported for SC, can only be satisfactorily predicted for a) a highly-staggered corneocyte geometry and b) corneocytes that are about 1000 times less permeable than the surrounding lipid phase.

The permeability calculation schemes developed by all the aforementioned models are based substantially on the

[1] National Center for Scientific Research "Demokritos," 15310 Ag. Paraskevi Attikis, Greece.

[2] Department of Chemical Engineering, National Technical University of Athens, 15780 Zografos, Greece.

[3] To whom correspondence should be addressed at NCSR "Demokritos," 15310 Ag. Parraskevi Attikis, Greece. (e-mail: stubos@avra@ipta.demokritos.gr)

ABBREVIATIONS: C_L, penetrant's concentration in the lipids; $C_{L,i}$, penetrant's concentration in the lipids across the lipid–protein interface; C_P, penetrant's concentration in the corneocytes; $C_{P,i}$, penetrant's concentration in the corneocytes across the lipid–protein interface; D_{eff}, overall effective diffusion coefficient; D_L, diffusion coefficient of stratum corneum's lipid phase; D_P, diffusion coefficient of stratum corneum's protein phase; I(Q), scattering intensity; l_x, corneocytes length; l_z, corneocyte thickness; l_p, dimension of lipid gap between corneocytes; Q, scattering vector; $R_z(r)$, auto-correlation function; S_1, one-point correlation function; $S_2(r)$, two-point correlation function; Z(x), phase function; $\gamma(r)$, correlation function at point r; ε, average fraction of diffusion area of the lipid phase on the skin surface; 2θ, scattering angle; κ, partition coefficient between the lipid and protein phases; λ, wavelength; ρ, scattering length density; σ, κ D_L/D_P; φ, porosity.

geometrical dimensions of SC biphasic structure. The pertinent actual sizes and dimensions may vary considerably from one skin sample to the next, depending on such factors as (i) anatomical location of the skin sample, (ii) subject-to-subject variability, (iii) internal structural integrity of the skin, and (iv) type of mammalian skin (5). Numerical estimates for the geometrical parameters of SC, which have to be considered as merely representative, suggest that corneocytes possess a lateral dimension, l_x, of approximately 30 μm and a longitudinal dimension, l_z, of approximately 1 μm, while the lamellar bilayer zones separating the corneocytes are approximately 0.05 μm in thickness l_p (11). A schematic diagram of the cross-section of SC is presented in Figure 1. Surprisingly, knowledge of the geometric SC biphasic structure, although improved over the last few years, is still relatively poor compared to its important functions. A wide range of methods have been employed, aiming to efficiently study the structure of either human or animal SC, e.g., thermal analysis (12) and Fourier transform infrared spectroscopy (13). Emphasis, however, has been given to the investigation of SC's lipid phase ultrastructure by the use of scattering techniques like small-angle X-ray scattering and wide-angle X-ray scattering. These methods proved to be really helpful for the structural and physicochemical characterization of a wide variety of materials, in particular porous media. Scattering data can generate important information regarding not only certain structural parameters, but also the dynamic properties of heterogeneous media.

One of the first attempts to demonstrate the feasibility of obtaining structural information using diffraction methods was reported in 1973 when Wilkes *et al.* (14) examined the SC structure using WAXD and thermal analysis. Later, Friberg and Osborne (15) published a brief account of SAXD studies of human SC, and White *et al.* (16) described a detailed SAXD and WAXD investigation of intact SC and extracted lipids, and isolated "couplets" from hairless mice. Bouwstra *et al.* (17,18) achieved significant progress, reinvestigating human and mouse SC and furthermore reporting the first studies of the lipid structure of porcine SC (19).

Recently, Very Small Angle Neutron Scattering (VSANS) was used for the first time to investigate the bulk properties of the intercellular region of porcine SC (20). Up to now, there have been neutron spectroscopy results reported that refer to an attempt of studying only monolayer and bilayer lipid systems, due to the extremely complex nature of the actual lipid structures existing within the SC (21). VSANS is a modern nondestructive technique, appropriate for providing information about scattering inhomogeneties as large as 1 μm. It is based on the same principles as SANS. A beam of neutrons is incident on a sample and the resultant pattern of scattered radiation intensity is examined. The outcome of such an experiment is a scattering curve showing the decay of the scattered intensity, I(Q), against the scattering vector, Q (20). Much of the information that can be gained from the obtained spectra is similar in nature to that produced by small-angle X-ray scattering. However, neutron scattering can often prove a more useful technique, especially in the context of pharmaceutical sciences. Neutrons, for example, are principally scattered by atomic nuclei and not electrons (as X-rays are). Hence, because the nucleus is a point scatterer, the scattered intensity does not decrease with increasing Q values. This is an important advantage in high resolution structural studies. Furthermore, different isotopes of an element may scatter neutrons differently; thus, using isotopic substitution, the scattering of chemically similar samples can be changed significantly (21).

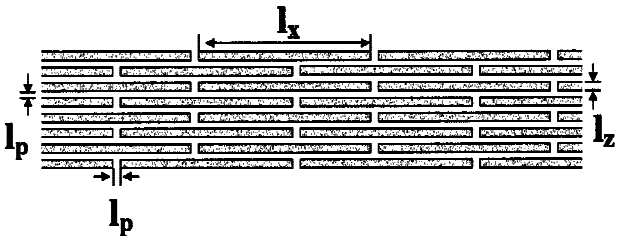

Fig. 1. The "brick-and-mortar" configuration of stratum corneum's cross-section. The characteristic dimensions shown are: the corneocyte length l_x, the corneocyte thickness l_z and the spacing between the corneocytes l_p, occupied by lipid bilayers.

In (20), the present authors suggested a qualitative mechanism for the description of the effect of hydration on SC structure, using the VSANS technique. It is the objective of this work to further interpret the SC VSANS spectra in order to obtain quantitative information about the dimensions of porcine SC biphasic geometrical configuration. A critical step in this attempt is the determination of the correlation function. It is well known that density fluctuations are the main origin of scattering. In the case of a biphasic medium, these fluctuations are localised at the interface which partitions the system (22). Thus, Small Angle Scattering (SAS) is strongly dependent on the geometrical properties of this oriented interface. SAS data have been frequently used for the indirect determination of biphasic media structural properties like correlation function (23), which gives a direct measure of the existing correlations at different scales of the mass distribution in the medium. In a further step, the results of the first part of this study are employed in an effort to numerically determine the effective diffusion coefficient of a substance through SC. The proposed approach aims at providing significant insight and data as a supplement to the experimental flux measurements that are currently the primary tools used to characterize transdermal solute transport. These macroscopic measurements are the only practical way to evaluate the potential efficiency of a transdermal drug delivery system and determine whether the achieved rate lies within the expected therapeutic limits. Due to experimental limitations and inherent uncertainties, significant discrepancies between reported experimental results occur in the literature (11), while such measurements by themselves can provide only limited insight into the relevant transport mechanisms.

Analysis and Interpretation of SANS Data

In the Small Angle Scattering (SAS) practice, either with neutrons (SANS) or X-rays (SAXS), most of the structural information is contained in the interval:

$$\pi/6 \leq Q \cdot d \leq 2\pi \quad (1)$$

where d is a characteristic dimension of the structure, and $Q = 4\pi\sin 2\theta/\lambda$, with 2θ denoting the scattering angle and λ denoting the wavelength. The SAS techniques can detect structural entities larger than 10 Å, with best results obtained for entities larger than 20 Å and smaller than 1 μm (24).

For an isotropic scatterer, the spherically averaged intensities I(Q) may be represented by the integral :

$$I(Q) = 4\pi\rho^2 V \int_0^\infty r^2 \gamma(r) \frac{\sin Qr}{Qr} dr \quad (2)$$

where V is the sample volume, ρ is the scattering length density, γ(r) is the density fluctuation auto-correlation function at point r, and Q is the scattering vector defined above. The above relation 2 shows how the intensity can be calculated as a function of the scattering angle provided the function γ(r) is known for all distances r. Conversely, using for instance the Fourier-inversion we can say that the density auto-correlation function can be calculated as a function of the distance, provided the intensity is known as a function of the angle.

The function γ(r) plays a role similar to the lattice structure of crystals (25). It defines the correlation length which can be considered as the characteristic length that provides a measure of the grain size in the medium. More specifically, the *n*-point correlation function is a measure of the probability of finding *n* points all lying in the region of space occupied by one constituent of a two-phase material. The phase function of the medium is defined as follows:

$$Z(x) = \begin{cases} 1 \text{ if x belongs to material 1} \\ 0 \text{ otherwise} \end{cases} \quad (3)$$

In most cases, knowledge of the first two moments of the medium's phase function is sufficient for the reliable reconstruction of a biphasic medium (26). The one-point correlation function S_1 is the probability that any point lies in phase 1 and is defined as:

$$S_1 = \langle Z(x) \rangle = \varphi \quad (4)$$

where the brackets indicate a volume average over the spatial coordinate x. Hence S_1 is equal to the volume fraction φ of phase 1 in the medium. In the case of the present SC structural study, φ, multiplied by 100, represents the corresponding fractional lipid content. On the other hand, the two-point correlation function $S_2(r)$, is the probability that two points a specified distance |r| apart, are both in phase 1 and is defined as:

$$S_2(r) = \langle Z(x) Z(x + r) \rangle \quad (5)$$

According to the definitions 3–5, it is straightforward to show that $S_2(0) = \varphi$ and $S_2(\infty) = \varphi^2$ (27). The two-point correlation function $S_2(r)$, is directly related to the aforementioned γ(r) (28), through the expression:

$$\gamma(r) = S_2(r) - \varphi^2 \quad (6)$$

In the present work, the VSANS scattering curves used have been obtained from the double crystal diffractometer V12a of Hahn-Meitner Institut, Berlin, at Q ranges between 0.006 and 0.04 nm^{-1}, employing four dry porcine SC samples from two different animals. The resulting scattering curves practically coincide in the Q-range of interest in this study ($Q > 0.01$ nm^{-1}). Their average (the uncertainty in the experimental I(Q) points of Figure 2a is estimated as ± 0.003 nm^{-1} for $Q > 0.01$ nm^{-1}) is mathematically transformed to produce the average two-point correlation function, $S_2(r)$, according to the Fourier-inversion procedure described above. The auto-correlation function (ACF), $R_z(r)$ is subsequently calculated (Figure 2b):

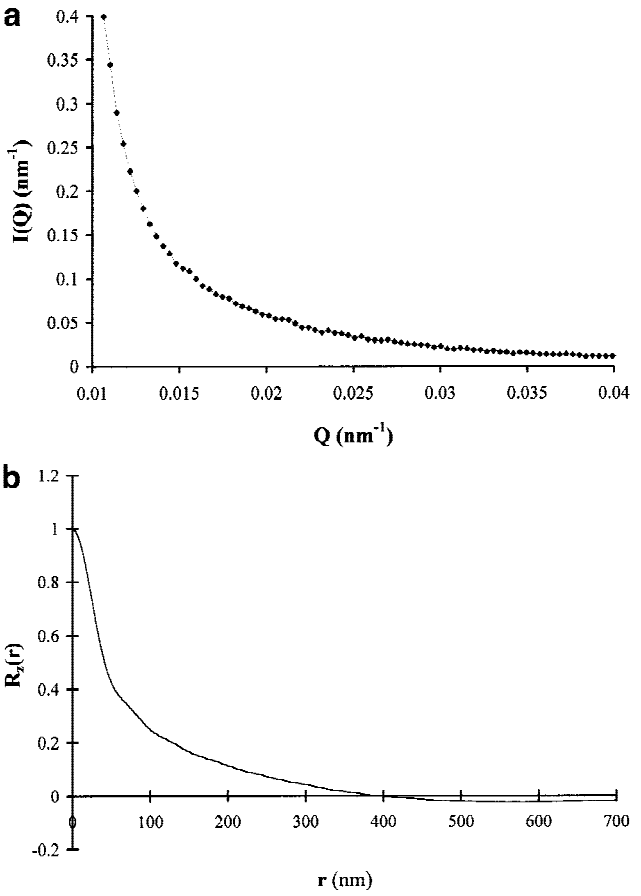

Fig. 2. (a) Very Small Angle Neutron Scattering spectrum of dry porcine stratum corneum. (b) Auto-correlation function resulting from the transformation of the VSANS spectrum, obtained from the dry porcine stratum corneum samples.

$$R_z(r) = \frac{S_2(r) - S_2(0)^2}{S_2(0) - S_2(0)^2} \quad (7)$$

It is then attempted to produce a structure for SC that matches the experimentally determined ACF. To this end, the biphasic "brick-and-mortar" geometry is adopted for the representation of SC structure (7,10) and a series of such two-dimensional SC domains, are constructed and digitized, by varying within certain realistic limits, the following dimensions: l_x = corneocyte length, l_z = corneocyte thickness, l_p = horizontal and vertical lipid gap between corneocytes (Figure 1).

For each generated domain, the corresponding average auto-correlation function is calculated according to a standard mathematical procedure described in detail elsewhere (27), and compared with the $R_z(r)$ curve obtained from the VSANS spectra, as shown in Figures 3–6. The variation of corneocyte length l_x between 20 and 40 μm, does not affect the original shape of the ACF (see Figure 3). This is because such length scales are clearly outside the range of the present SAS, and thus their effect on the ACF curve cannot be detected. Turning to structural parameters with sizes within the SAS range tested, it is observed that no appreciable effects on

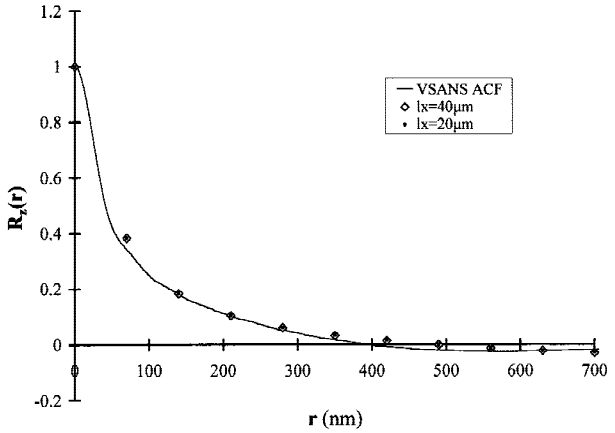

Fig. 3. Effect of corneocyte length l_x variation on auto-correlation function. The other dimensions have standard values: $l_z = 0.8$ μm and $l_p = 0.07$ μm.

the ACF are caused when the corneocyte thickness l_z varies between 0.6 and 1 μm (Figure 4), or the lipid dimension l_p varies between 0.05 and 0.075 μm (Figure 5). On the contrary, significant deviations from the reference VSANS ACF occur for $l_z = 2$ μm and for l_p values greater than 0.1 μm or smaller than 0.05 μm (see Figures 4 and 5, respectively). Hence, it follows that when simulating porcine SC structure based on the standard "brick-and-mortar" model, the most appropriate values for l_z and l_p dimensions, according to the present analysis, are $0.6 < l_z < 1$ μm and $0.05 < l_p < 0.1$ μm, respectively. These results seem to compare very well with previous indirect suggestions of the literature (5,6,11).

In addition, following Tojo's (8) approach for a more realistic representation of the SC structure, a "random brick" case is established by varying the geometric parameters of the SC model structure, according to a Gaussian distribution function, with the following mean values and standard deviations:

$$\langle l_x \rangle = 40\ \mu m,\ \sigma_{lx} = 10\%$$
$$\langle l_z \rangle = 0.8\ \mu m,\ \sigma_{lz} = 10\%$$
$$l_p = 0.07\ \mu m$$

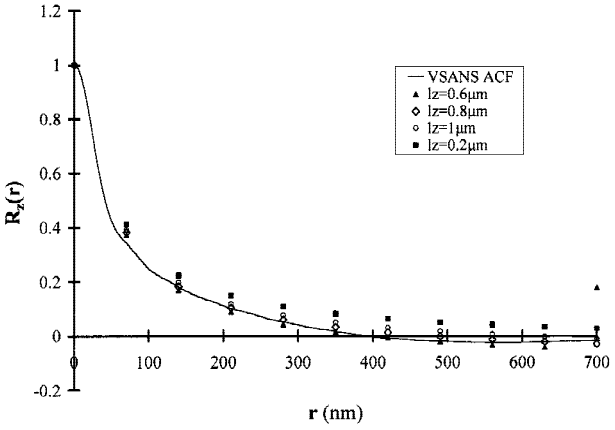

Fig. 4. Effect of corneocyte thickness l_z variation on auto-correlation function. The other dimensions have standard values: $l_x = 40$ μm and $lp = 0.07$ μm. No appreciable effects on the ACF are detected when l_z varies between 0.6 and 1 μm, while significant deviations occur when $l_z = 2$ μm.

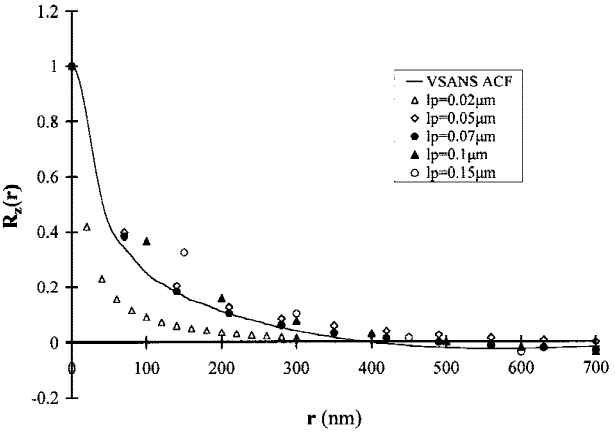

Fig. 5. Effect of lipid dimension l_p variation on auto-correlation function. The other dimensions have standard values: $l_x = 40$ μm and $l_z = 0.8$ μm. No appreciable effects on the ACF are detected when lp varies between 0.05 and 0.075 μm, while significant deviations occur for l_p values greater than 0.1 μm or smaller than 0.05 μm.

As expected from the above results, the correlation function of this "random brick" structure presented in Figure 6, shows no significant deviation from the experimental ACF curve. Indeed the limits of l_x and l_z variations are such that, according to the previous paragraph, should not cause appreciable changes in the ACF curve of this Tojo-like randomised SC picture. This does not necessarily imply that the actual randomness of SC structure is to be automatically neglected, when investigating its transport properties.

Modeling of Porcine Stratum Corneum Diffusion Properties

The SC barrier properties to a permeating substance strongly depend on its internal geometry. Following the above conclusions on porcine SC structural parameters, an effort is made to estimate the effective diffusion coefficient D_{eff}, through SC domains exhibiting an ACF in good agreement with the experimental one. For this purpose, the steady-state diffusion equation is numerically solved employing finite differences on unstructured grids. The diffusion is considered to take place through both the corneocytes and the intercellular region. The key parameters for the estimation of D_{eff} for a specific substance through the model SC domain are: a) the

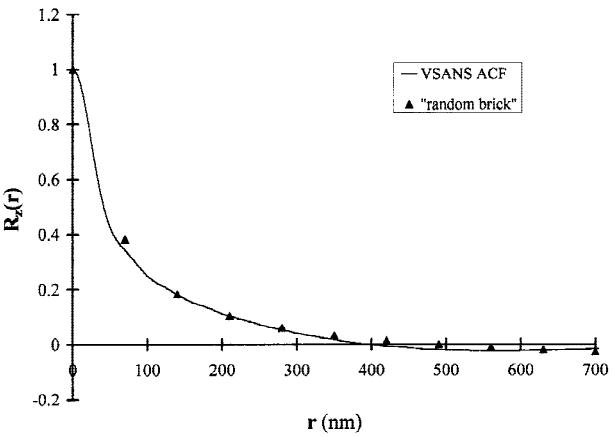

Fig. 6. Auto-correlation function curve for a domain with "random brick" structure.

geometrical configuration of the domain, b) the relative diffusivity of the lipid and corneocyte phases, given by the quotient D_L/D_P and c) the solute physicochemical behavior in terms of the partition coefficient κ, between the lipid and protein phase. The product $\kappa D_L/D_P$ defines the dimensionless quantity σ. The overall diffusivity on digitized "brick-and-mortar" media is determined by solving the steady state diffusion equation in each phase. When considering steady-state, the transient term of Fick's second law becomes zero and the following expression, known as Laplace equation is derived:

$$D_{eff}\,\nabla^2 C = 0 \tag{8}$$

A second-order finite difference scheme, similar to the one used by Thovert *et al.* in random media and regular fractals (29) is used to solve Laplace equation in two dimensions. Because of the large-scale periodicity of the SC structure, the mass transfer problem is solved by considering a computational domain, consisting of three rectangular corneocytes within each of 15 parallel layers, with periodic conditions on the left and right boundaries. Fixed concentrations are imposed at the top and bottom boundaries. Specifically, the following expressions 9 and 10, corresponding to the lipid and protein phase respectively, are employed:

$$D_L\left[\frac{\partial^2 C_L}{\partial x^2}+\frac{\partial^2 C_L}{\partial y^2}\right]=0 \tag{9}$$

$$D_P\left[\frac{\partial^2 C_P}{\partial x^2}+\frac{\partial^2 C_P}{\partial y^2}\right]=0 \tag{10}$$

where C_L and C_P denote the solute concentration in the lipid and the protein phase respectively. The coupling between equations 9 and 10 is made through the use of the partition coefficient, $\kappa = C_{L,i}/C_{P,i}$ where $C_{L,i}$ and $C_{P,i}$ represent the concentration values just across the lipid–protein interface. The succesive-overrelaxation method turned out to be very effective for the present problem. Each run on a PC Pentium II required approximately 0.5–4 hr of CPU time depending on the input conditions.

It is important to note that unstructured grids are used to cope with the highly different length scales involved in each SC phase in accordance with the work of Heisig *et al.* (10). In particular, a much finer grid is built on the lipid side of the lipid–protein interface due to the very large difference in relevant sizes ($l_p << l_z << l_x$). This gradual transition from the fine lipid phase mesh to its coarser counterpart in the protein phase, and proved to be necessary for convergence of the concentration solution at the pertinent interface.

Figure 7 illustrates a set of curves corresponding to calculated D_{eff}/D_L ratio for σ values ranging from 10^{-3} to 10^5 and for domains with different geometry configurations. Since the auto-correlation function analysis of the previous section provided only the optimum l_z and l_p ranges (due to its insensitivity to l_x dimension variations), one could consider that information on proper values of l_x may be obtained by fitting calculated overall diffusivities to experimental data. To this end, in this section, we mainly focus on studying the effect of l_x upon the diffusion characteristics of the system under investigation. Specifically, two domains of the same l_z and l_p values (equal to 0.8 μm and 0.07 μm respectively) and different l_x values are examined.

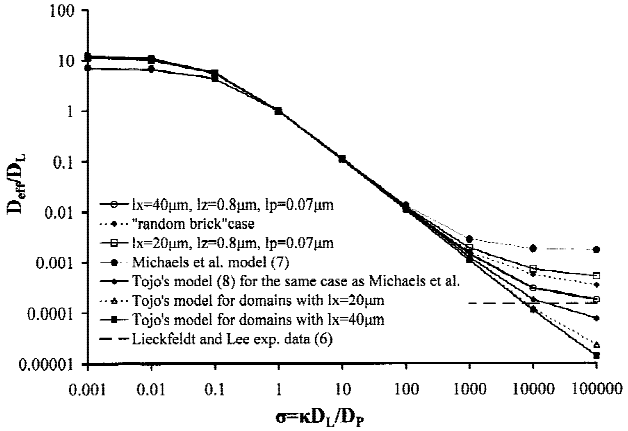

Fig. 7. Calculated D_{eff}/D_L values for model stratum corneum domains with different geometry (focus on the effect of corneocyte thickness, l_x, variation). Comparison with experimental data and analytical models.

For σ values greater than about 1000, the active agent diffuses preferably through the intercellular region. In this case, the decrease of the corneocyte longitudinal dimension l_x from 40 μm to 20 μm results in a more than threefold increase of D_{eff}/D_L. These numerically obtained results can be compared with those of Lieckfeldt and Lee (6). They first measured drug diffusivity, D_L, in a structured matrix composed of model SC lipids. Although their reported values depend on lipid composition, they were all within the range 10^{-9}–10^{-8} cm^2/s and should be considered as spatially-averaged over all existing bilayer orientations. The effective diffusivity, D_{eff}, within excised human SC, was then determined by the same authors from experimental permeation data. From these two measurements, they calculate an experimental ratio D_{eff}/D_L of 1.5×10^{-4}. As indicated in Figure 7, good agreement between this result and the present analysis is obtained for the case of "long" corneocyte "bricks" (domain with $l_x = 40$ μm, $l_z = 0.8$ μm and $l_p = 0.07$ μm).

For values of σ around unity, the medium behaves as a homogeneous structure since both phases are almost equally permeable (resulting values D_{eff}/D_L in Figure 7 close to unity as well). When the lipid-protein relative diffusivity σ varies from 0.1 to 1000, the value of D_{eff}/D_L changes by three or more orders of magnitude. However, in this range of σ the variation of l_x does not present any significant effect upon the effective diffusion coefficient. Decreasing the ratio σ below 0.1, we observe that D_{eff}/D_L values level off and that, again, the l_x variation (from 40 μm to 20 μm) gives no appreciable change of the effective diffusivity.

The randomised SC structure (in a Tojo-like manner (8)), gives also in Figure 7, D_{eff}/D_L values that lie, as expected, between the curves for $l_x = 20$ μm and $l_x = 40$ μm.

Note that the anisotropy of the lipid phase may result in different lateral and transbilayer diffusion coefficients inside this phase (5,10,11). Lateral diffusion within the lipid region accounts for diffusion along the bilayer plane ($D_\parallel$), while transbilayer transport involves the discontinuous process of solute diffusion across the bilayer plane ($D_\perp$) (11). Presently no sensitivity study of lateral/transbilayer diffusion effect has been conducted due to the lack of appropriate experimental data on $D_\parallel$, $D_\perp$. However the effect of decreasing $D_\perp$ com-

pared to D‖ should manifest itself in the low σ range of Figure 7. In our case, the deduction of l_x (~40 μm) is made from data concerning very high σ-values where the effect of D⊥<<D‖ is negligible.

It is interesting to compare the present numerical calculations with the simplified analytical expressions developed by Michaels *et al.* (7) and Tojo (8). This comparison is also presented in Figure 7. For σ values less than about 5.10^{-2}, the two analytical predictions lie close to the results of the present analysis. However, it is seen that the predictions of Michaels *et al.* overestimate the effective diffusivity considerably in the high σ range. In the same region, Tojo's predictions are lower than the numerical computations, a fact that may be attributed to a disproportionally weighted diffusion route through the lipid phase that Tojo used to develop his expression. As a result, Tojo's model can be easily shown to tend towards the asymptote $\varepsilon^2\sigma$ (ε denotes the average fraction of the lipid phase diffusion area on the skin surface) for high enough σ values, thus becoming unrealistically dependent on ε in that σ range. This leads to the severe underestimation of D_{eff} shown in Figure 7 for the SC configurations that have been qualified as best matching the VSANS data reported above.

CONCLUSIONS

Appropriate mathematical transformation of VSANS spectra provides valuable information about the biphasic geometrical configuration of porcine SC, in terms of the corresponding correlation function. By adopting the 2-dimensional brick-and-mortar model, an attempt is made to produce SC model structures that match the experimentally determined auto-correlation function (ACF).

The most appropriate values for the dimensions of the corneocyte thickness and the surrounding lipid gap, are found to lie in the range 0.6–1 μm and 0.05–0.1 μm respectively. The effect of corneocyte length variation cannot however be detected, because length scales of such magnitude are clearly outside the SAS resolution range of the present study.

As the SC barrier properties to a permeating substance relate to its internal geometry, the above conclusions on porcine SC structural parameters are further used for the calculation of the effective diffusivity D_{eff}, through the model domains exhibiting an ACF that fits best to the VSANS experimental data. The key parameter for the estimation of D_{eff} is the dimensionless quantity σ, which is a function of the partition coefficient and the relative diffusivity of the lipid and protein phases. The diffusion study focuses on the investigation of the effect of corneocyte length l_x upon the system's transport characteristics. It is shown that the effective SC diffusivity is inversely related to corneocyte size. Comparison with experimental data supports the validity of the results and indicates that the corneocyte length l_x is around 40 μm. The present numerical calculations are also compared with simplified analytical expressions developed by Michaels *et al.* (7) and Tojo (8). In the high σ-range, the predictions of Michaels *et al.* overestimate the effective diffusivity while Tojo's model leads to a severe underestimation of D_{eff}.

Summarizing, the suggested analysis highlights the relevance and efficiency of independent characterization methods, such as neutron scattering in its very small angle version, to provide evidence about SC's structural features. The resulting geometrical values can serve as a useful tool when SC's barrier properties are studied in relation to its heterogeneous morphology, especially when the "bricks-and-mortar" model is adopted. Discrepancies should however be expected, due to the variability of skin's physiology, as already mentioned in the introductory section of this study. Furthermore, the new methodology can be used for 'reconstructing' not only the intact structure of SC but also its deformation during certain transdermal drug delivery applications (e.g., hydration effect). The numerical model developed to describe the diffusion mechanism through SC offers flexibility with regard to geometric and other (physicochemical) parameters, capability to model 'random structures,' and amenability to future extensions including forced flow of the solute (due e.g., to sonophoresis or iontophoresis).

ACKNOWLEDGMENT

Support from the EPET II Programme of the General Secretariat for Research and Technology (EKVAN Contract No 146), Greece, BENSC at Hahn-Meitner Institut, Berlin-Germany and the European Commission (TMR Contract ERBFMGECT950060) is acknowledged.

REFERENCES

1. B. G. Amsden and M. F. A. Goosen. Transdermal delivery of peptide and protein drugs: An overview. *AIChE J.* **41**:1972–1997 (1995).
2. R. J. Scheuplein. Mechanisms of percutaneous absorption: I. Routes of penetration and the influence of solubility. *J. Invest. Dermatol.* **45**:334–346 (1965).
3. R. J. Scheuplein. Mechanism of percutaneous absorption: II. Transient diffusion and the relative importance of various routes of skin penetration. *J. Invest. Dermatol.* **48**:79–88 (1967).
4. J. W. Albery and J. Hadgraft. Percutaneous absorption: in vivo experiments. *Pharm. Pharmacol.* **31**:140–147 (1979).
5. D. A. Edwards and R. Langer. A linear theory of transdermal transport phenomena. *J. Pharm. Sci.* **83**:1315–1334 (1994).
6. R. Lieckfeldt and G. Lee. Use of a model lipid matrix to demonstrate the dependence of the stratum corneum's barrier properties on its internal geometry. *J. Contr. Rel.* **20**:183–194 (1992).
7. A. S. Michaels, S. K. Chandrasekaran, and J. E. Shaw. Drug permeation through human skin: Theory and *in vitro* experimental measurement. *AIChE J.* **21**:985–996 (1975).
8. K. Tojo. Random brick model for drug transport across stratum corneum. *J. Pharm. Sci.* **76**:889–891 (1987).
9. J. W. Albery and J. Hadgraft. Percutaneous absorption: Theoretical description. *Pharm. Pharmacol.* **31**:129–139 (1979).
10. M. Heisig, R. Lieckfeldt, G. Wittum, G. Mazurkevich, and G. Lee. Non-steady-state descriptions of drug permeation through stratum corneum. I. The biphasic brick-and-mortar model. *Pharm. Res.* **13**:421–426 (1996).
11. M. E. Johnson, D. Blankschtein, and R. Langer. Evaluation of solute permeation through the stratum corneum: Lateral bilayer diffusion as the primary transport mechanism. *J. Pharm. Sci.* **86**: 1162–1172 (1997).
12. G. M. Golden, D. B. Guzek, A. H. Kennedy, J. E. McKie, and R. O. Potts. Stratum corneum lipid phase transitions and water barrier properties. *Biochemistry* **26**:2382–2388 (1987).
13. R. O. Potts, D. B. Guzek, R. R. Harrism, and J. E. McKie. A noninvasive, in vivo technique to quantitative measure water concentration of the stratum corneum using attenuated total-reflectance infrared spectroscopy. *Arch. Dermatol. Res.* **277**:489–495 (1985).
14. G. L. Wilkes, A. L. Nguyen, and R. Wildnauer. Structure-property relations of human and neonatal rat stratum corneum. I. Thermal stability of the crystalline lipid structure as studied by X-ray diffraction and differential thermal analysis. *Biochim. Biophys. Acta* **304**:267–275 (1973).
15. S. E. Friberg and D. W Osborne. Small-angle X-ray diffraction

patterns of stratum corneum and a model structure for its lipids. *J. Dispersion Sci. Tech.* **6**:485–495 (1985).
16. S. H. White, D. Mirejovsky, and G. I. King. Structure of lamellar lipid domains and corneocyte envelopes of murine stratum corneum. An X-ray diffraction study. *Biochemistry* **27**:3725–3732 (1988).
17. J. A. Bouwstra, G. S. Gooris, J. A. van der Spek, and W. Bras. Structural investigations of human stratum corneum by small-angle X-ray scattering. *J. Invest. Dermatol.* **97**:1005–1012 (1991).
18. J. A. Bouwstra, G. S. Gooris, J. A. Van der Spek, S. Lavrijsen, and W. Bras. The lipid and protein structure of mouse stratum corneum: A wide- and small angle diffraction study. *Biochim. Biophys. Acta* **1212**:183–192 (1994).
19. J. A. Bouwstra, G. S. Gooris, W. Bras, and D. T. Downing. Lipid organisation in pig stratum corneum. *J. Lipid. Res.* **36**:685–695 (1995).
20. G. Ch. Charalambopoulou, Th. A. Steriotis, A. Ch. Mitropoulos, K. L. Stefanopoulos, N. K. Kanellopoulos, and A. Ioffe. Investigation of water sorption on porcine stratum corneum by very small angle neutron scattering. *J. Invest. Dermatol.* **110**:988–990 (1998).
21. A. C. Watkinson, J. Hadgraft, P. R. Street, and R. W. Richards. Neutrons, Surfaces, and Skin. In R. O. Potts and R. H. Guy (eds.), *Mechanisms of Transdermal Drug Delivery,* Marcel Dekker, New York, 1997, pp. 231–265.
22. P. Levitz and D. Tchoubar. Disordered porous solids: from chord distributions to small angle scattering. *J. Phys. I France* **2**:771–790 (1992).
23. J. M. Drake and J. Klafter. Dynamics of confined molecular systems. *Physics Today* **May**:46–55 (1990).
24. A. Ch. Mitropoulos, K. Beltsios, Th. A. Steriotis, F. K. Katsaros, P. Makri, and N. K. Kanellopoulos. The combination of equilibrium and dynamic methods for the detailed structural characterisation of ceramic membranes. *J. Europ. Cer. Soc.* **18**:1545–1558 (1998).
25. P. Debye, H. R. Anderson Jr. and H. Brumberger. Scattering by an inhomogeneous solid. II. The correlation function and its applications. *J. Appl. Phys.* **28**:679–683 (1957).
26. J. Yao, P. Frykman, F. Kalaydjian, J. F. Thovert, and P. M. Adler. High-order moments of the phase function for real and reconstructed model porous media: A comparison. *J. Colloid Interface Sci.* **156**:478–490 (1993).
27. J. G. Berryman. Measurement of spatial correlation functions using image processing techniques. *J. Appl. Phys.* **57**:2374–2384 (1985).
28. P. Levitz, G. Ehret, S. K. Sinha, and J. M. Drake. Porous Vycor glass: The microstrucrure as probed by electron microscopy, direct energy transfer, small angle scattering, and molecular adsorption. *J. Chem. Phys.* **95**:6151–6161 (1991).
29. J. F. Thovert, F. Wary, and P. M. Adler. Thermal conductivity of random media and regular fractals. *J. Appl. Phys.* **68**:3872–3883 (1990).